Supplementary material

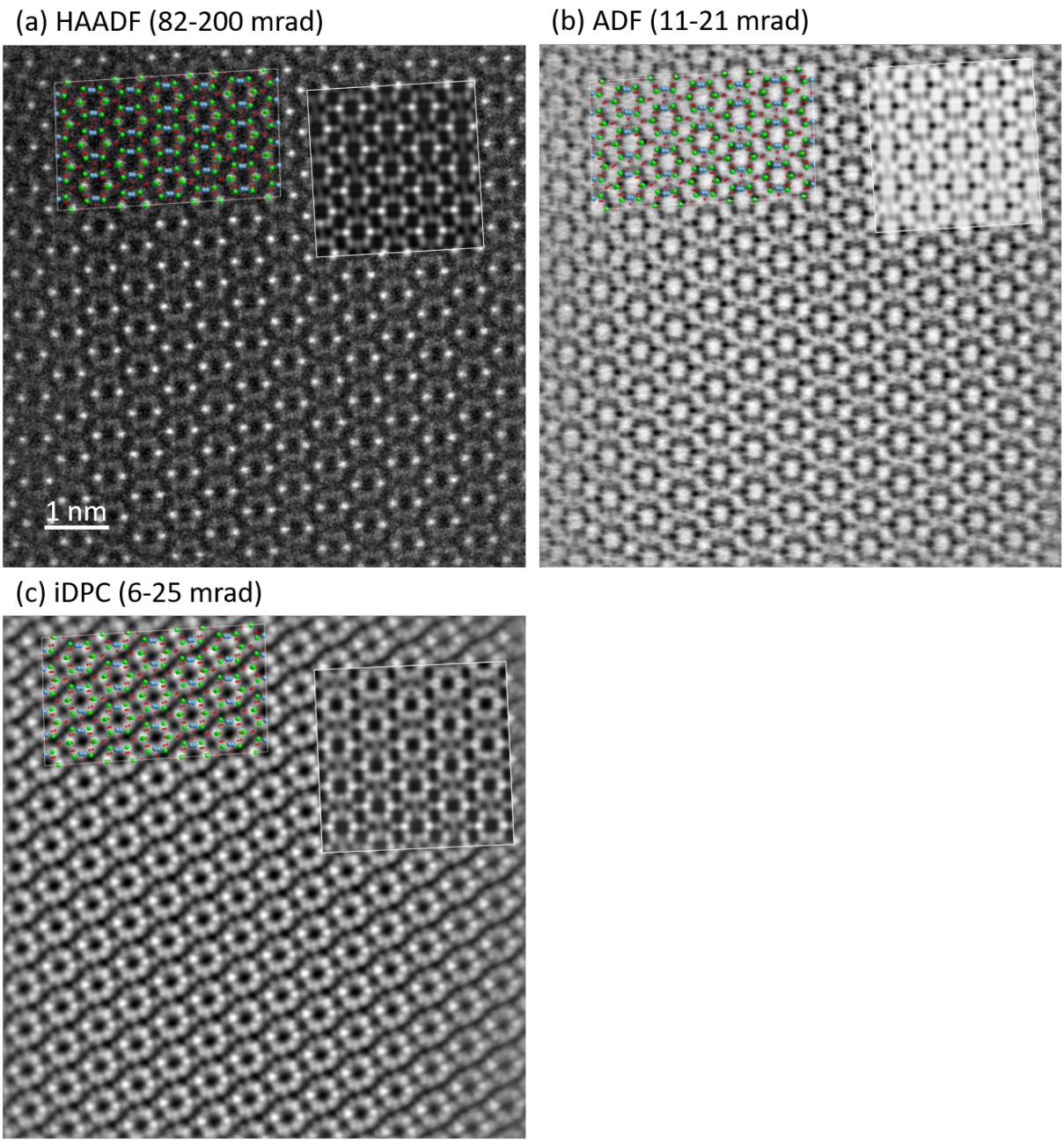

Fig. S1. (a) High angle annular dark field (HAADF), (b) annular dark field (ADF) with collection angles 11-21 mrad, (c) integrated differential phase contrast (iDPC) with collection angles 6-25 mrad scanning electron transmission electron microscopy (STEM) of plagioclase along PL[001]. The crystal structure of plagioclase is superimposed on top of each acquisition according to the atomic column correspondence. The corresponding simulated images are shown as insets in the top right corner.

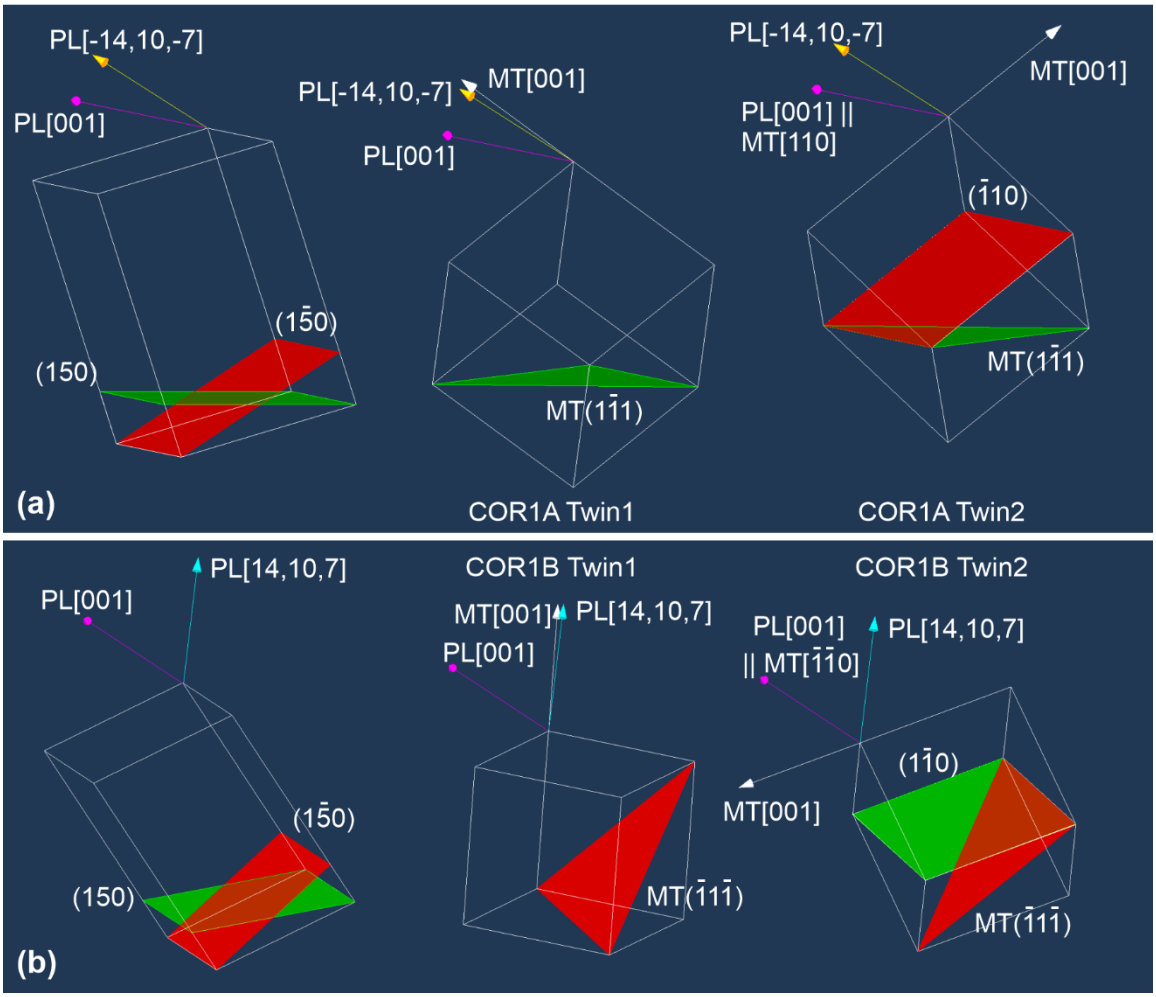

Fig. S2. (a) COR1A between plagioclase and magnetite unit cells. PL[001], PL[-14,10,-7], PL(150) and PL(1$\bar{5}$0) are shown in the plagioclase unit cell. Magnetite unit cell COR1A twin 1 shows correspondence between PL[001] || MT[$\bar{1}\bar{1}$0], PL(150) || MT(1$\bar{1}$1) and PL[-14,10,-7] || MT[001] with a small deviation. Magnetite unit cell COR1A twin 2 shows correspondence between PL[001] || MT[110], PL(150) || MT(1$\bar{1}$1) and PL(1$\bar{5}$0) || MT($\bar{1}$10). (b) COR1B between plagioclase and magnetite unit cells. PL[001], PL[14,10,7], PL(150) and PL(1$\bar{5}$0) are shown in the plagioclase unit cell. Magnetite unit cell COR1B twin 1 shows correspondence between PL[001] || [110], PL(1$\bar{5}$0) || MT($\bar{1}$1$\bar{1}$) and PL[14,10,7] || MT[001] with a small deviation. Magnetite unit cell COR1B twin 2 shows correspondence between PL[001] || MT[$\bar{1}\bar{1}$0], PL(1$\bar{5}$0) || MT($\bar{1}$1$\bar{1}$) and PL(150) || MT(1$\bar{1}$0).

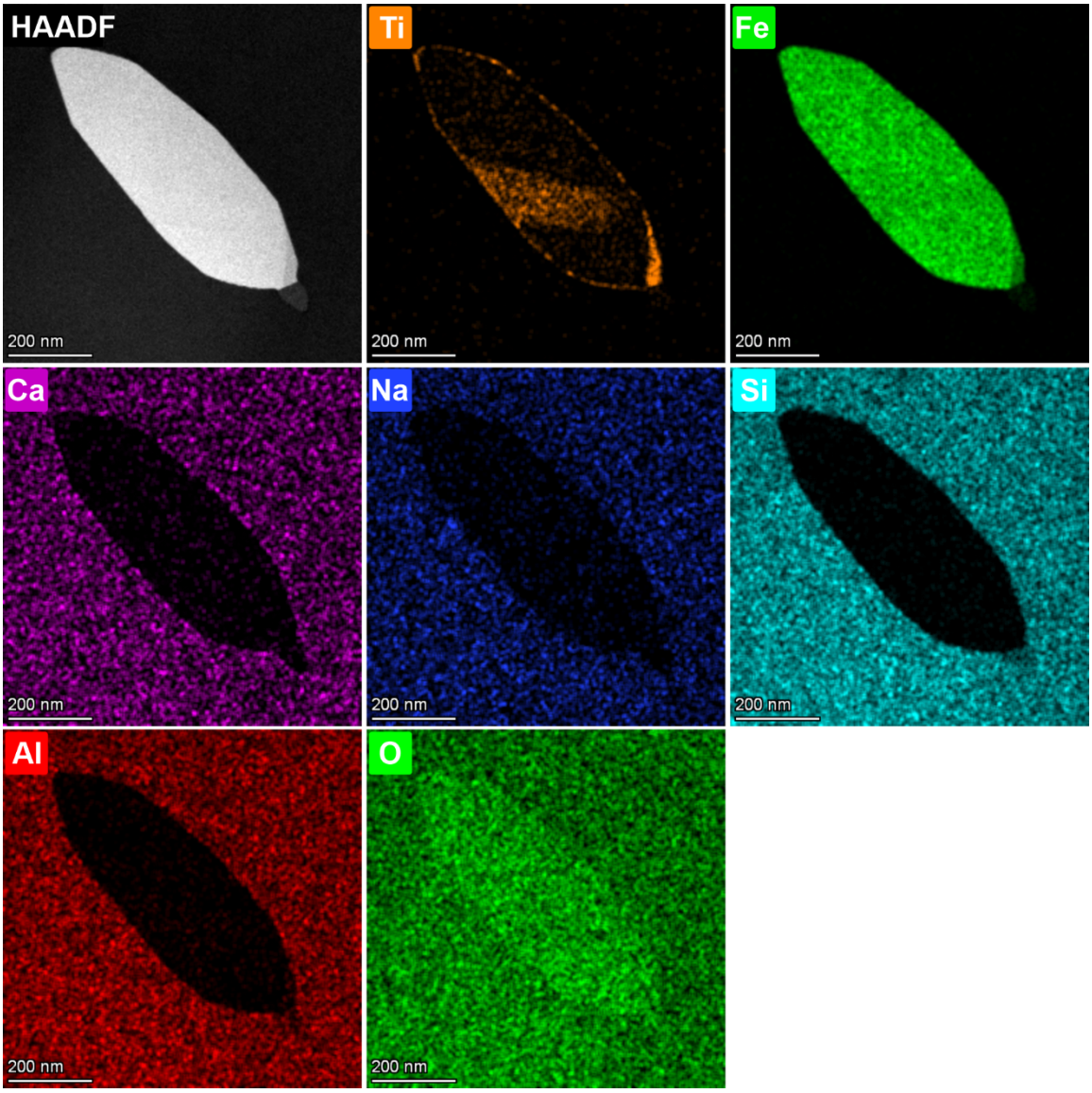

Fig. S3. STEM-EDS elemental distribution maps of the cross-section of a COR1A PL[001]-MT micro-inclusion in main orientation. The inclusion is magnetite containing a Ti-rich phase in the central area. The second phase is most likely ulvospinel according to the cubic symmetry. A Ti-rich rim is observed along the magnetite-plagioclase interface.

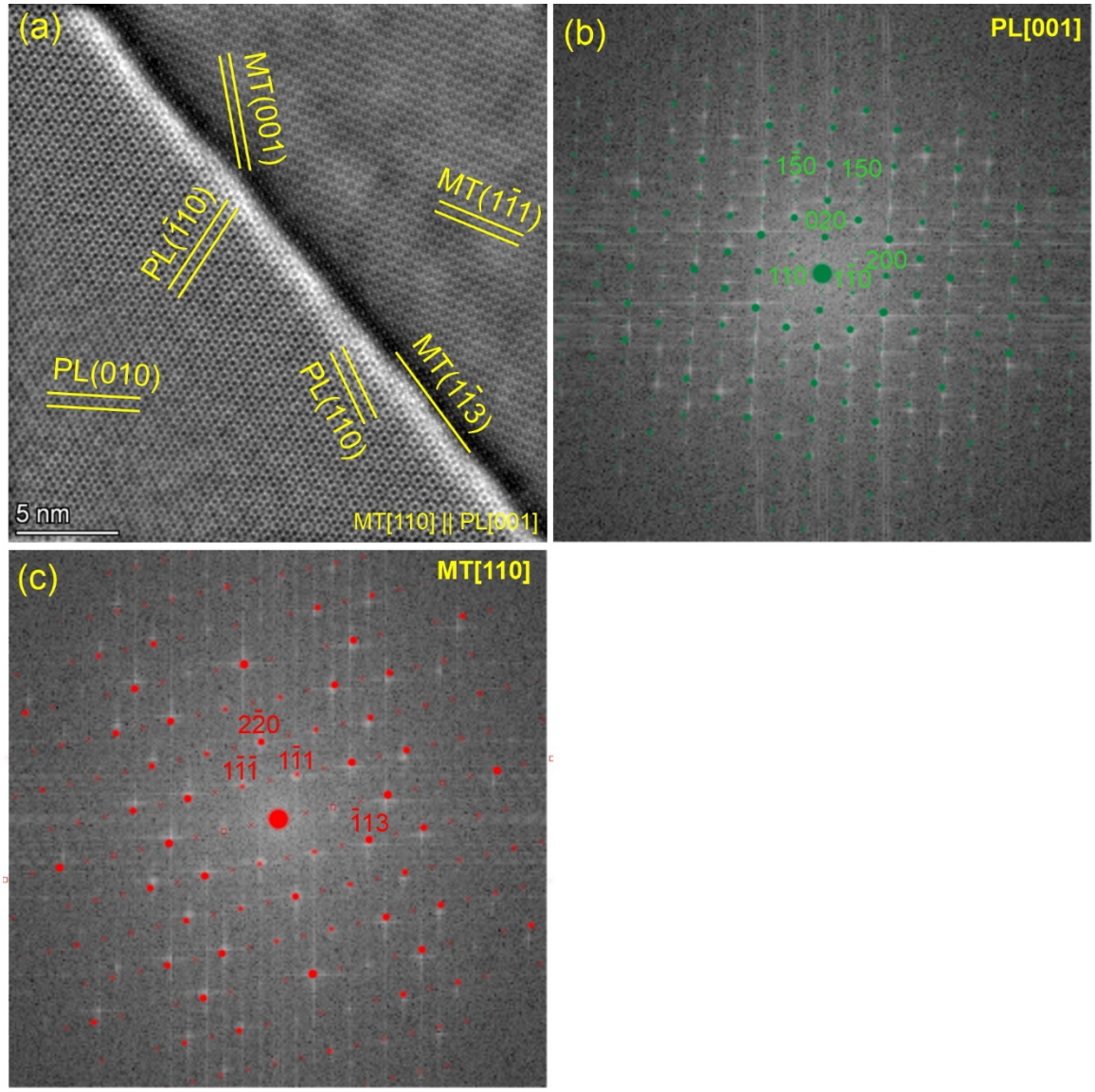

Fig. S4. (a) iDPC-STEM image of an interface segment of the magnetite-plagioclase interface of a COR1A PL[001]-MT micro-inclusion in main orientation. Viewing direction is MT[110] || PL[001]. Lattice fringes in magnetite and in plagioclase are highlighted and indexed. (b) Fast Fourier transformation (FFT) of the plagioclase area in (a). The simulated diffraction pattern of plagioclase (green dots) according to the orientation in (a) is superimposed. Representative diffraction spots representing the lattice planes in plagioclase in reciprocal space are indexed with green Miller indices nearby. (c) FFT of the magnetite area in (a). Simulated diffraction pattern of magnetite (red dots) according to the orientation in (a) is superimposed. Representative diffraction spots representing the lattice planes in magnetite in reciprocal space are indexed with red Miller indices nearby.

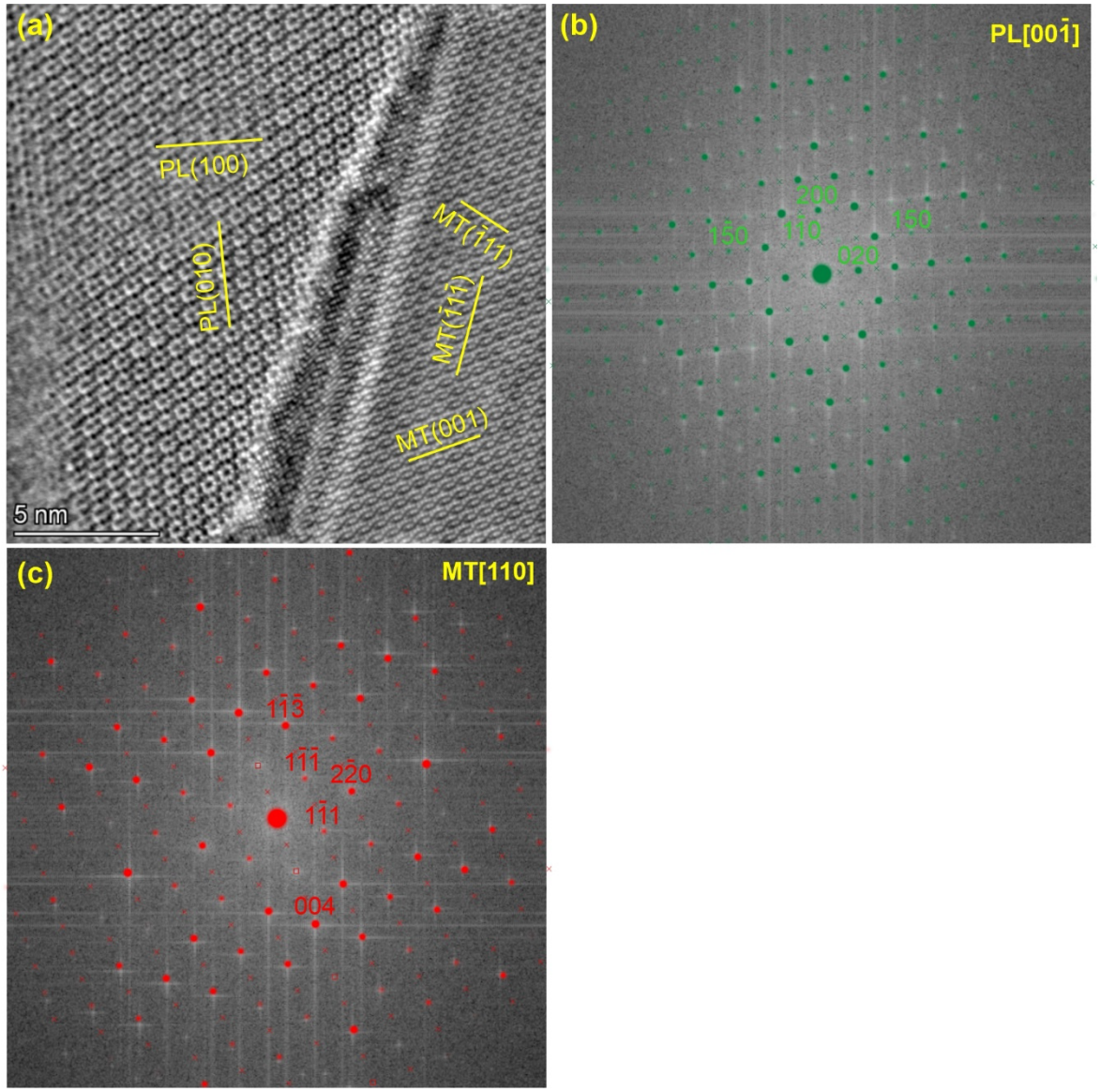

Fig. S5. (a) iDPC-STEM of an interface segment of the magnetite-plagioclase interface of a COR1B PL[001]-MT micro-inclusion in main orientation. Viewing direction is MT[110] || PL[00$\bar{1}$]. Lattice fringes in magnetite and in plagioclase are highlighted and indexed. (b) Fast Fourier transformation (FFT) of the plagioclase area in (a). Simulated diffraction pattern of plagioclase (green dots) according to the orientation in (a) is superimposed. Representative diffraction spots representing the lattice planes in plagioclase in reciprocal space are indexed with green Miller indices nearby, (c) FFT of the magnetite area in (a). Simulated diffraction pattern of magnetite (red dots) according to the orientation in (a) is superimposed. Representative diffraction spots representing the lattice planes in magnetite in reciprocal space are indexed with red Miller indices nearby.